

# Thermal dielectron measurements in Au+Au collisions at $\sqrt{s_{NN}} = 7.7, 14.6, \text{ and } 19.6 \text{ GeV}$ with the STAR experiment

Yiding Han (Rice University)  
for the STAR Collaboration

**Abstract.** Dielectrons emitted during the evolution of the hot and dense QCD medium created in relativistic heavy-ion collisions offer an effective way to probe the medium properties, as they do not interact via the strong force. The rate of the dielectron emission is proportional to the medium's electromagnetic spectral function. In the dielectron invariant mass range from  $400 \text{ MeV}/c^2$  to  $800 \text{ MeV}/c^2$ , the spectral function probes the in-medium  $\rho$  meson propagator which is sensitive to the medium's properties including the total baryon density and the temperature. Meanwhile, the low energy range of the spectral function provides information about the medium's electrical conductivity. Therefore, by measuring thermal dielectron production, we can study the microscopic interactions between the electromagnetic current and the medium. The STAR experiment has recorded large datasets of Au+Au collisions during the Beam Energy Scan Phase-II (BES-II) program, spanning center-of-mass energies between  $\sqrt{s_{NN}} = 3.0$  and  $19.6 \text{ GeV}$  with detector upgrades that benefit the dielectron measurement via extended transverse momentum and rapidity coverages as well as enhanced particle identification capability. In these proceedings, we will report on the measurements of thermal dielectrons produced in Au+Au collisions at  $\sqrt{s_{NN}} = 7.7, 14.6, \text{ and } 19.6 \text{ GeV}$  using the STAR experiment.

## 1 Introduction

Heavy-ion collisions emit thermal radiation at each stage, encompassing both the Quark-Gluon Plasma (QGP) phase and the hadronic phase. This radiation allows us to investigate various properties of the QCD medium formed during these collisions. Key among these are the interactions between electromagnetic (EM) currents and the medium, as well as the evolution of the fireball. Experimentally, this thermal radiation can be detected through dilepton production.

The rate of dilepton production in thermal radiation is determined by a confluence of factors: the lepton phase-space factor, the thermal Bose-Einstein distribution, and the electromagnetic spectral function [1, 2]. Model calculations show that for dileptons in the intermediate mass range (with  $M_\phi < M_{ll} < M_{J/\psi}$ ), the EM current predominantly exhibits partonic behavior [3]. Conversely, in the low mass range (with  $M_{ll} < 1 \text{ GeV}/c^2$ ), the current is dominated by vector mesons [9]. Essentially, the EM spectral function is a blend of the imaginary components of vector meson propagators, predominantly influenced by the isospin effect, manifesting as  $\rho$ -dominance [4].

To examine how the medium temperature and total baryon density impact the EM spectral function, the STAR experiment is conducting thermal dielectron measurements. These are

being carried out at lower collision energies (between  $\sqrt{s_{NN}} = 3$  and 19.6 GeV) from the Beam Energy Scan Phase-II (BES-II). This phase features advanced detector capabilities and enhanced statistics, facilitating more accurate observations.

## 2 Experiment and analysis

The data presented in these proceedings were obtained using the STAR detector at the RHIC during the years 2019 and 2021. These data are taken from Au+Au collisions at collision energies of  $\sqrt{s_{NN}} = 19.6, 14.6,$  and 7.7 GeV. The number of events, meeting stringent quality criteria, amounted to 200 million at 19.6 GeV, 120 million at 14.6 GeV, and 37 million at 7.7 GeV. The 2019 19.6 GeV data has an approximate factor of 10 increase in sample size compared to the data collected during the Beam Energy Scan Phase-I (BES-I) in 2010-2014.

Electron identification within the STAR framework primarily utilizes the combination of two detector subsystems: the Time Projection Chamber (TPC) which is instrumental in determining track momentum and ionization energy loss ( $dE/dx$ ), and the Time of Flight (TOF) system which is vital for measuring the velocity of charged particles.

Dielectron signal processing begins with the construction of a  $e^+e^-$  continuum, formed by pairing all possible combinations of electrons and positrons from the same event. We estimate the combinatorial and correlated background by employing the acceptance-corrected geometric mean of like-sign pairs. The acceptance discrepancy between unlike- and like-sign pairs is estimated using the mixed-event technique[5–8].

Subtracting the background spectrum from the dielectron  $e^+e^-$  continuum yields the raw signal. The raw spectrum is then adjusted for detector inefficiencies. A comprehensive exposition of the dielectron signal reconstruction process is detailed in [5]. The physical background (cocktail including hadronic decays and Drell-Yan process) for the thermal radiation dielectron production includes the following channels:  $DY \rightarrow e^-e^+, D\bar{D} \rightarrow e^-e^+\nu_e\bar{\nu}_eX, J/\psi \rightarrow e^-e^+, \pi^0(\eta, \eta') \rightarrow \gamma e^-e^+, \omega \rightarrow \pi^0 e^-e^+, \omega \rightarrow e^-e^+, \phi \rightarrow \eta e^-e^+, \phi \rightarrow e^-e^+$ .

The efficiency correction for the dielectron spectrum encompasses both single-track electron reconstruction efficiency and the dielectron loss at  $M_{ee} < 0.2$  GeV/c<sup>2</sup> due to photon conversion removal. The methodology for efficiency calculation is the same as the approach described in [6].

## 3 Results and discussion

The efficiency-corrected invariant mass spectra, presented in Fig. 1, correspond to the 0-80% most-central Au+Au collisions at  $\sqrt{s_{NN}} = 19.4, 14.6,$  and 7.7 GeV. In Fig. 1, the blue points represent the invariant mass spectra within the STAR acceptance at mid-rapidity ( $|\eta^e| < 1, p_T^e > 0.2$  GeV/c,  $|y^{ee}| < 1$ ), where the vertical blue lines indicate statistical uncertainty, and the blue boxes denote the systematic uncertainty for each data point. The experimental data are juxtaposed with the physics background processes, depicted as a solid black line with an accompanying grey band representing uncertainty, following the same methodology as described in [5–8].

Figure 2 displays the detector acceptance-corrected excess yield, calculated as,

$$\text{Excess yield} = (\text{Efficiency corrected data} - \text{background processes})/\text{Acceptance} \quad (1)$$

Acceptance is the detector-acceptance correction. The acceptance correction employs a virtual photon method described in [7]. Panel (a) of Fig. 2 contrasts the excess yield invariant mass spectra from RHIC BES-I (triangles) and BES-II (circles) at  $\sqrt{s_{NN}} = 19.6$  GeV, affirming consistency between the two measurements. Additionally, due to enhanced statistics and

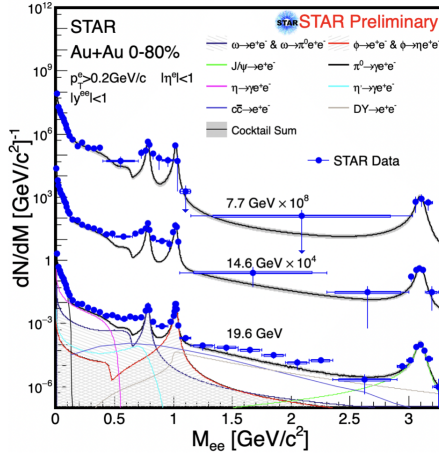


**Figure 1.** Efficiency-corrected dielectron invariant mass spectrum within the STAR acceptance for Au+Au at  $\sqrt{s_{NN}} = 19.6, 14.6,$  and  $7.7$  GeV. Experimental results with statistical and systematic uncertainties are shown as points. The physical background is illustrated with solid lines.

detector upgrades in BES-II, the total error is reduced by a factor of 4 compared to BES-I. Panel (b) of Fig. 2 depicts the excess yield invariant mass spectra from BES-II across various collision energies (19.6, 14.6, and 7.7 GeV, from top to bottom), with the 19.6 GeV excess yield closely aligning with the Rapp model's predictions [9] for the same system and collision energy. The decreasing yield with lower collision energies at low mass range underscores medium effects on the EM spectral function, including increased total baryon density and reduced average medium temperature at lower collision energies.

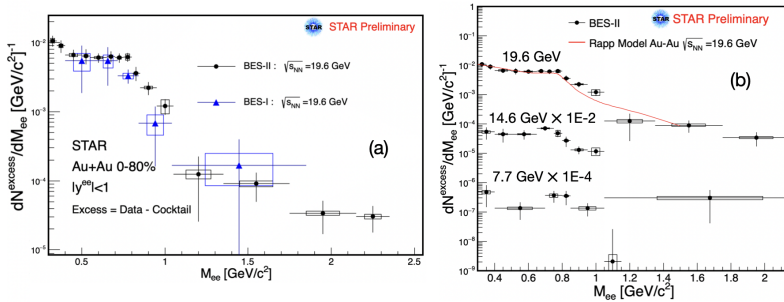


**Figure 2.** (a) Acceptance-corrected excess yield invariant mass spectra for Au+Au  $\sqrt{s_{NN}} = 19.6$  GeV, with statistical and systematic uncertainties. For comparison, BES-I data are shown as triangles[7], and BES-II data as circles. (b) BES-II acceptance-corrected excess yield invariant mass spectra at Au+Au  $\sqrt{s_{NN}} = 19.6, 14.6,$  and  $7.7$  GeV (points), compared with the Rapp model at Au+Au  $\sqrt{s_{NN}} = 19.6$  GeV (solid line).

Figure 3 features the integrated excess yield, for  $0.4 < M_{ll} < 0.75$  GeV/c<sup>2</sup>, normalized by the  $\pi^0$  yield (estimated as  $N_{\pi^0} = \frac{N_{\pi^+} + N_{\pi^-}}{2}$ ). This figure combines results from multiple experiments: STAR BES-II (red stars) and BES-I (blue stars) [7, 8] in 0-80% centrality Au+Au collisions, alongside data from NA60 (black crosses) [10] and HADES (black squares) [11]

experiments. The experimental results are compared to the Rapp model's predictions (pink open circles). STAR BES-II's new findings bridge the gap between the BES-I and HADES results, suggesting a downward trend in the normalized integrated excess yield from high to low collision energies, which may provide constraints for models describing medium interactions.

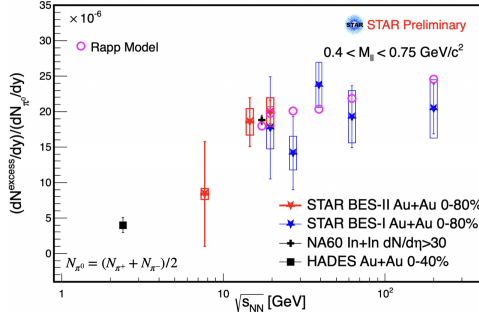


**Figure 3.** Integrated excess yield from different experiments for  $0.4 < M_{II} < 0.75 \text{ GeV}/c^2$ , normalized by the  $\pi^0$  yield. The open circles represent the Rapp model's calculations.

## 4 Summary

In this study, we presented thermal dielectron invariant mass spectra obtained from STAR BES Phase-II Au+Au collisions at  $\sqrt{s_{NN}} = 7.7, 14.6, \text{ and } 19.6 \text{ GeV}$ . The data from the 19.6 GeV collisions, benefiting from high statistical quality, align well with predictions based on the hadronic many-body approach for the electromagnetic spectral function. The varying invariant mass spectra observed at 14.6 and 7.7 GeV illuminate the influence of medium conditions, particularly the total baryon density and medium temperature, on the EM spectral function.

In addition, STAR's new observations of the integrated excess yield hint at a decreasing trend from higher to lower  $\sqrt{s_{NN}}$  values. This trend not only provides new insights into the dynamics of the medium created in heavy-ion collisions but also offers potential constraints for theoretical models aimed at describing the complex interactions within this medium.

## References

- [1] E. L. Feinberg, *Nuovo Cim. A* **34**, 391 (1976).
- [2] L. D. McLerran and T. Toimela, *Phys. Rev. D* **31**, 545 (1985).
- [3] E. Braaten, R. D. Pisarski, T.-C. Yuan, *Phys. Rev. Lett.* **64**, 2242 (1990).
- [4] J. J. Sakurai, **Currents and Mesons** (University of Chicago Press, Chicago, 1969).
- [5] A. Adare et al. (PHENIX Collaboration), *Phys. Rev. C* **81**, 034911 (2010).
- [6] L. Adamczyk et al. (STAR Collaboration), *Phys. Rev. C* **92**, 024912 (2015).
- [7] L. Adamczyk et al. (STAR Collaboration), *Phys. Lett. B* **750**, 64 (2015).
- [8] M. I. Abdulhamid et al. (STAR Collaboration), *Phys. Rev. C* **107**, L061901 (2023).
- [9] H. van Hees and R. Rapp, *Phys. Rev. Lett.* **97**, 102301 (2006).
- [10] R. Arnaldi et al. (NA60 Collaboration), *EPJ C* **59**, 607 (2009).
- [11] J. Adamczewski-Musch et al. (HADES Collaboration), *Nat. Phys.* **15**, 1040–1045 (2019)